may also explain the larger extent of quiet Sun spicules[1,2] where p-mode power and granular flows are stronger by up to 50% and magnetic fields are more inclined owing to the presence of opposite polarity[24,25].

A natural consequence of our model is that the quasi-periodic shocks driving the spicules propagate upwards into the low corona, where they may lead to intensity oscillations with properties that are similar to those of longitudinal oscillations observed by TRACE[26] in 1 MK coronal loops[27]. □

Received 31 March; accepted 14 June 2004; doi:10.1038/nature02749.

1. Beckers, J. M. Solar spicules. *Sol. Phys.* **3,** 367–433 (1968).
2. Beckers, J. M. Solar spicules. *Annu. Rev. Astron. Astrophys.* **10,** 73–100 (1972).
3. Sterling, A. C. Solar spicules: a review of recent models and targets for future observations. *Sol. Phys.* **196,** 79–111 (2000).
4. Withbroe, G. L. The role of spicules in heating the solar atmosphere: implications of EUV observations. *Astrophys. J.* **267,** 825–836 (1983).
5. Foukal, P. *Solar Astrophysics* 10–11 (John Wiley & Sons, New York, 1990).
6. De Pontieu, B., Erdélyi, R. & de Wijn, A. G. Intensity oscillations in the upper transition region above active region plage. *Astrophys. J.* **595,** L63–L66 (2003).
7. Roberts, B. The resonant response to granular buffeting. *Sol. Phys.* **61,** 23–34 (1979).
8. Hollweg, J. V. On the origin of solar spicules. *Astrophys. J.* **257,** 345–353 (1982).
9. Sterling, A. C. & Hollweg, J. V. The rebound shock model for solar spicules—Dynamics at long times. *Astrophys. J.* **327,** 950–963 (1988).
10. Sterling, A. C. & Hollweg, J. V. A rebound shock model for solar fibrils. *Astrophys. J.* **343,** 985–993 (1989).
11. Sterling, A. C. & Mariska, J. T. Numerical simulations of the rebound shock model for solar spicules. *Astrophys. J.* **349,** 647–655 (1990).
12. Suematsu, Y., Wang, H. & Zirin, H. High-resolution observation of disk spicules: I. Evolution and kinematics of spicules in the enhanced network. *Astrophys. J.* **450,** 411–421 (1995).
13. Spruit, H. C. & Roberts, B. Magnetic flux tubes on the sun. *Nature* **304,** 401–406 (1983).
14. Scharmer, G. B., Bjelksjö, K., Korhonen, T. K., Lindberg, B. & Pettersson, B. in *Innovative Telescopes and Instrumentation for Solar Astrophysics* (eds Keil, S. & Avakyan, S.) 341–350 (Proc. SPIE, Vol. 4853, SPIE—The International Society for Optical Engineering, Hawaii, 2003).
15. James, S. P., Erdélyi, R. & De Pontieu, B. Can ion-neutral damping help to form spicules? *Astron. Astrophys.* **406,** 715–724 (2003).
16. Vernazza, J. E., Avrett, E. H. & Loeser, R. Structure of the solar chromosphere. III—Models of the EUV brightness components of the quiet-sun. *Astrophys. J. Suppl.* **45,** 635–725 (1981).
17. Schrijver, C. J. & Harvey, K. L. The photospheric magnetic flux budget. *Sol. Phys.* **150,** 1–18 (1994).
18. Scherrer, P. H. *et al.* The Solar Oscillations Investigation—Michelson Doppler Imager. *Sol. Phys.* **162,** 129–188 (1995).
19. Christensen-Dalsgaard, J., Gough, D. & Toomre, J. Seismology of the Sun. *Science* **229,** 923–931 (1985).
20. Cheng, Q.-Q. & Yi, Z. Oscillations in the solar atmosphere: a result of hydrodynamical simulations. *Astron. Astrophys.* **313,** 971–978 (1996).
21. Sutmann, G. & Ulmschneider, P. Acoustic wave propagation in the solar atmosphere: II. Nonlinear response to adiabatic wave excitation. *Astron. Astrophys.* **294,** 241–251 (1995).
22. Museliak, Z. E. & Ulmschneider, P. Atmospheric oscillations in solar magnetic flux tubes. I. Excitation by longitudinal waves and random pulses. *Astron. Astrophys.* **400,** 1057–1064 (2003).
23. Carlsson, M. & Stein, R. F. Does a nonmagnetic solar chromosphere exist? *Astrophys. J.* **440,** L29–L32 (1995).
24. Schrijver, C. J. & Title, A. M. The magnetic connection between the solar photosphere and the corona. *Astrophys. J.* **597,** L165–L168 (2003).
25. Schrijver, C. J. *et al.* A new view of the solar outer atmosphere by the transition region and coronal explorer. *Sol. Phys.* **187,** 261–302 (1999).
26. Handy, B. N. *et al.* The transition region and coronal explorer. *Sol. Phys.* **187,** 229–260 (1999).
27. De Moortel, I., Ireland, J., Walsh, R. W. & Hood, A. W. Longitudinal intensity oscillations in coronal loops observed with TRACE — I. Overview of measured parameters. *Sol. Phys.* **209,** 61–88 (2002).
28. Lindsey, C. *et al.* Extreme-infrared brightness profile of the solar chromosphere obtained during the total eclipse of 1991. *Nature* **358,** 308–310 (1992).
29. De Pontieu, B., Tarbell, T. D. & Erdélyi, R. Correlations on arcsecond scales between chromospheric and transition region emission in active regions. *Astrophys. J.* **590,** 502–518 (2003).
30. Rae, I. C. & Roberts, B. Pulse propagation in a magnetic flux tube. *Astrophys. J.* **256,** 761–767 (1982).

Acknowledgements This work was supported by NASA, the UK Particle Physics Research Council (PPARC) and NSF Hungary. The Swedish Solar Telescope is operated on the island of La Palma by the Royal Swedish Academy of Sciences in the Spanish Observatorio del Roque de los Muchachos of the Instituto de Astrofisica de Canarias. R.E. thanks M. Kéray for encouragement. We thank C.J. Schrijver, T. Tarbell, M. DeRosa and A. Title for discussions, and M. Carlsson for pointing out the importance of 3 min oscillations.

Competing interests statement The authors declare that they have no competing financial interests.

Correspondence and requests for materials should be addressed to B.D.P. (bdp@lmsal.com).

A universal scaling relation in high-temperature superconductors

C. C. Homes[1], S. V. Dordevic[1], M. Strongin[1], D. A. Bonn[2], Ruixing Liang[2], W. N. Hardy[2], Seiki Komiya[3], Yoichi Ando[3], G. Yu[4], N. Kaneko[5]*, X. Zhao[5], M. Greven[5,6], D. N. Basov[7] & T. Timusk[8]

[1]*Department of Physics, Brookhaven National Laboratory, Upton, New York 11973, USA*
[2]*Department of Physics and Astronomy, University of British Columbia, Vancouver, British Columbia V6T 2A6, Canada*
[3]*Central Research Institute of Electric Power Industry, Komae, Tokyo 201-8511, Japan*
[4]*Department of Physics, Stanford University, Stanford, California 94305, USA*
[5]*Stanford Synchrotron Radiation Laboratory, Stanford, California 94309, USA*
[6]*Department of Applied Physics, Stanford University, Stanford, California 94305, USA*
[7]*Department of Physics, University of California at San Diego, La Jolla, California 92093, USA*
[8]*Department of Physics and Astronomy, McMaster University, Hamilton, Ontario L8S 4M1, Canada*

* Present address: National Institute of Advanced Industrial Science and Technology, Tsukuba Central 2-2, Tsukuba, Ibaraki 305-8568, Japan

Since the discovery of superconductivity at elevated temperatures in the copper oxide materials[1] there has been a considerable effort to find universal trends and correlations amongst physical quantities, as a clue to the origin of the superconductivity. One of the earliest patterns that emerged was the linear scaling of the superfluid density (ρ_s) with the superconducting transition temperature (T_c), which marks the onset of phase coherence. This is referred to as the Uemura relation[2], and it works reasonably well for the underdoped materials. It does not, however, describe optimally doped (where T_c is a maximum) or overdoped materials[3]. Similarly, an attempt to scale the superfluid density with the d.c. conductivity (σ_{dc}) was only partially successful[4]. Here we report a simple scaling relation ($\rho_s \propto \sigma_{dc}T_c$, with σ_{dc} measured at approximately T_c) that holds for all tested high-T_c materials. It holds regardless of doping level, nature of dopant (electrons versus holes), crystal structure and type of disorder[5], and direction (parallel or perpendicular to the copper–oxygen planes).

We first demonstrate scaling for the *a*–*b* plane (that is, parallel to the copper–oxygen planes) properties[6–12] of single- and double-layer copper oxide materials (Supplementary Table 1), as well as for the conventional metals[13,14] Nb and Pb (elemental superconductors with relatively high values of T_c). The values for ρ_s and σ_{dc} are obtained simultaneously from studies of the reflectance of these materials. The results for the scaling relation are shown on a log–log plot in Fig. 1. The dashed line is a linear fit to the data, while the dotted lines form what are effectively an upper and lower bound for the data; this is described by $\rho_s = (120 \pm 25)\sigma_{dc} T_c$ (where ρ_s is in cm^{-2}, σ_{dc} is in $\Omega^{-1}\,cm^{-1}$, and T_c is in K). The remarkable result contained in this plot is that within error all of these points fall onto a single line with a slope of unity. This is significant, as the optimally and overdoped materials, which fall well off of the Uemura plot, now scale with the underdoped materials onto a single line.

We also searched for scaling relations along the poorly conducting *c* axis, where the charge transport is thought to be incoherent[15]. Previous work focused on scaling between ρ_s and σ_{dc} only[16,17]. Whereas this approach yields good results for the underdoped materials, in a fashion reminiscent of the Uemura plot, significant deviations from linearity are encountered for optimally and overdoped materials; this was thought to signal the onset of more conventional three-dimensional behaviour. Figure 2 demonstrates

that the *c*-axis data[11,17–20] for all of the single and double-layer materials (Supplementary Table 2) are again well described by a line with slope of unity. What is perhaps most remarkable is that the *a*–*b*-plane and *c*-axis results may all be described by the same universal line shown in Fig. 2, even though the two results correspond to very different ranges of ρ_s. The combined data span nearly five orders of magnitude, from the insulating behaviour along the *c* axis in the underdoped systems, to the metallic behaviour in the *a*–*b* planes of the overdoped copper oxides.

The scaling relation for the *a*–*b* planes can be interpreted in a number of different ways. One of the most direct is the assumption that all of the spectral weight (the area obtained from the integral of the optical conductivity) associated with the free-carriers of the normal state (n_n) collapses into the superconducting condensate[21] ($n_s \equiv n_n$) below T_c. Allowing that the low-frequency conductivity at $T \approx T_c$ can be described by the simple Drude theory for a metal, $\sigma_1(\omega) = \sigma_{dc}/(1 + \omega^2\tau^2)$ (where ω is frequency), which has the shape of a lorentzian centred at zero frequency with a width at half-maximum given by the scattering rate $1/\tau$, the area under this curve may be approximated simply as σ_{dc}/τ. Transport measurements for the copper oxides[22] suggest that $1/\tau$ near the transition scales linearly with T_c, so the strength of the condensate is just $\rho_s \propto \sigma_{dc} T_c$, in agreement with the observed scaling relation. This result requires that these materials approach the clean limit ($1/\tau \ll 2\Delta$, where 2Δ is the superconducting energy gap).

However, this approach cannot be applied to the properties along the *c* axis, because it is generally conceded that transport in this direction is incoherent, and therefore hopping rather than scattering governs the physics[15]. The quasi-two-dimensional nature of the copper oxides, which often includes a semiconducting or activated response of the resistivity along the *c* axis, has motivated the description of the superconductivity in this direction in terms of a Josephson-coupling picture[16,17,23–26]. The *c*-axis penetration depth λ is then determined by the Josephson current density J_c and is $\lambda^2 = \hbar c^2/8\pi deJ_c$, where $J_c = (\pi\Delta/2eR_n)\tanh(\Delta/2k_BT)$, d is the separation between the planes, and $R_n = d/\sigma_{dc}$ is the normal-state tunnelling resistance[24]. There is convincing evidence that the energy gap in the copper oxides is *d*-wave in nature, containing nodes at the Fermi surface[27,28], making the determination of J_c difficult. However, if the coupling between the planes originates at the (0,π), (π,0) points[29] where the gap is a maximum, Δ_0, then we can approximate $\Delta \approx \Delta_0$. Furthermore, if $\Delta_0 \propto T_c$, then $J_c \propto T_c/R_n$ and $\rho_s \propto \sigma_{dc}T_c$, which yields the observed scaling behaviour in the *c*-axis direction. Despite the different nature of the transport properties parallel and perpendicular to the *a*–*b* planes, the universal scaling pertaining to both directions is an unusual and surprising result that should provide new insights into the origins of the superconductivity in these materials. □

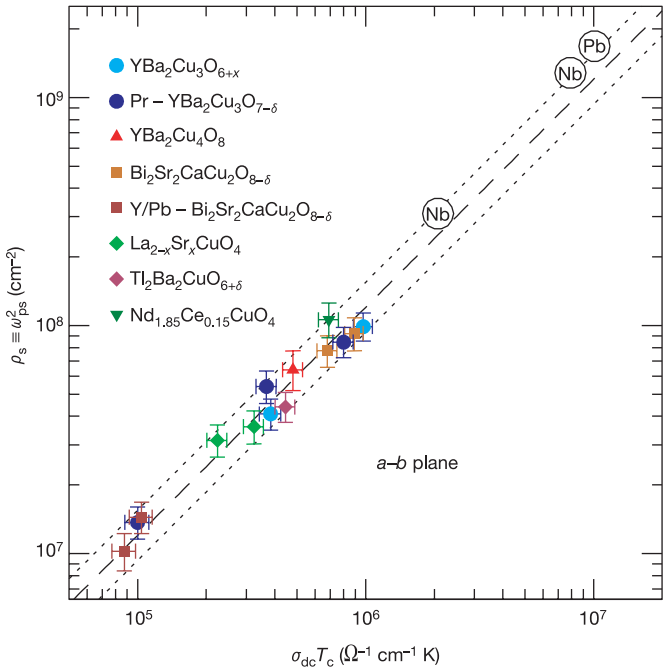

Figure 1 Plot of the superfluid density (ρ_s) versus the product of the d.c. conductivity (σ_{dc}) and the superconducting transition temperature (T_c) for a variety of copper oxides and some simple metals. (σ_{dc} is measured just above the transition, and parallel to the copper–oxygen (*a*–*b*) planes; data are shown on a log–log plot; see Supplementary Table 1 for details, including errors.) The values for σ_{dc} and ρ_s are obtained from optical measurements of the reflectance. The reflectance is a complex quantity consisting of an amplitude and a phase; in an experiment only the amplitude is usually measured. However, if the reflectance is measured over a wide frequency range, the Kramers–Kronig relation may be used to obtain the phase. Once the complex reflectance is known, then other complex optical functions may be calculated (for example, the dielectric function or the conductivity). The σ_{dc} used in this scaling relation has been extrapolated from the real part of the optical conductivity $\sigma_{dc} = \sigma_1(\omega \rightarrow 0)$ at $T \approx T_c$. For $T \ll T_c$, the response of the dielectric function to the formation of a condensate is expressed purely by the real part, $\epsilon_1(\omega) = \epsilon_\infty - \omega_{ps}^2/\omega^2$, which allows the superconducting plasma frequency ω_{ps} to be calculated from $\omega_{ps}^2 = -\omega^2\epsilon_1(\omega)$ in the $\omega \rightarrow 0$ limit, where $\omega_{ps}^2 = 4\pi n_s e^2/m^*$ is proportional to the number of carriers in the condensate. The strength of the condensate (ρ_s) is simply $\rho_s \equiv \omega_{ps}^2$. The dashed and dotted lines are described by $\rho_s = (120 \pm 25)\sigma_{dc}T_c$. Within error, all the data for the copper oxides are described by the dashed line. The data for the conventional superconductors Nb and Pb, indicated by the atomic symbols within the circles, lie slightly above the dashed line.

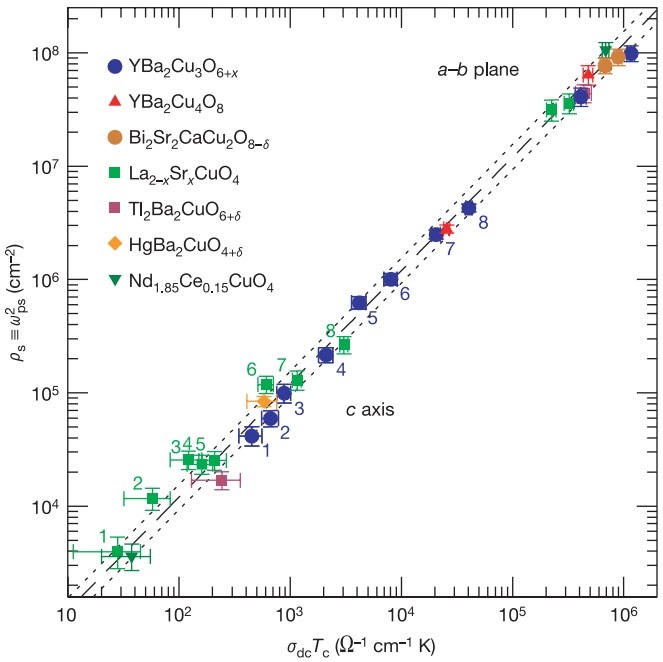

Figure 2 As Fig. 1 but for copper oxides only, and including data for the poorly conducting *c* axis. The values for ρ_s and σ_{dc} are obtained from optical measurements, as described in Fig. 1 legend. In addition to the published results, new data are also included for $HgBa_2CuO_{4+\delta}$ and $La_{2-x}Sr_xCuO_4$. Within error, all of the data fall on the same universal (dashed) line with slope of unity, defined by $\rho_s = 120\sigma_{dc}T_c$; the dotted lines are from $\rho_s = (120 \pm 25)\sigma_{dc}T_c$. See Supplementary Table 2 for details, including errors.

Received 20 February; accepted 17 May 2004; doi:10.1038/nature02673.

1. Bednorz, J. G. & Müller, K. A. Possible high T_c superconductivity in the Ba-La-Cu-O system. *Z. Phys. B* **64,** 189–193 (1986).
2. Uemura, Y. J. *et al.* Universal correlations between T_c and n_s/m^* (carrier density over effective mass) in high-T_c cuprate superconductors. *Phys. Rev. Lett.* **62,** 2317–2320 (1989).
3. Niedermayer, C. *et al.* Muon spin rotation study of the correlation between T_c and $n_s/_m{}^*$ in overdoped $Tl_2Ba_2CuO_{6+\delta}$. *Phys. Rev. Lett.* **71,** 1764–1767 (1993).
4. Pimenov, A. *et al.* Universal relationship between the penetration depth and the normal-state conductivity in YBCO. *Europhys. Lett.* **48,** 73–78 (1999).
5. Eisaki, H. *et al.* Effect of chemical inhomogeneity in bismuth-based copper oxide superconductors. *Phys. Rev. B* **69,** 064512 (2004).
6. Basov, D. N. *et al.* In-plane anisotropy of the penetration depth in $YBa_2Cu_3O_{7-x}$ and $YBa_2Cu_4O_8$ superconductors. *Phys. Rev. Lett.* **74,** 598–601 (1995).
7. Homes, C. C. *et al.* Effect of Ni impurities on the optical properties of $YBa_2Cu_3O_{6+x}$. *Phys. Rev. B* **60,** 9782–9792 (1999).
8. Liu, H. L. *et al.* Doping-induced change of optical properties in underdoped cuprate superconductors. *J. Phys. Condens. Matter* **11,** 239–264 (1999).
9. Puchkov, A. V., Timusk, T., Doyle, S. & Herman, A. M. *ab*-plane optical properties of $Tl_2Ba_2CuO_{6+\delta}$. *Phys. Rev. B* **51,** 3312–3315 (1995).
10. Homes, C. C., Clayman, B. P., Peng, J. L. & Greene, R. L. Optical properties of $Nd_{1.85}Ce_{0.15}CuO_4$. *Phys. Rev. B* **56,** 5525–5534 (1997).
11. Singley, E. J., Basov, D. N., Kurahashi, K., Uefuji, T. & Yamada, K. Electron dynamics in $Nd_{1.85}Ce_{0.15}CuO_{4+\delta}$: Evidence for the pseudogap state and unconventional c-axis response. *Phys. Rev. B* **64,** 224503 (2001).
12. Startseva, T. *et al.* Temperature evolution of the pseudogap state in the infrared response of underdoped $La_{2-x}Sr_xCuO_4$. *Phys. Rev. B* **59,** 7184–7190 (1999).
13. Pronin, A. V. *et al.* Direct observation of the superconducting energy gap developing in the conductivity spectra of niobium. *Phys. Rev. B* **57,** 14416–14421 (1998).
14. Klein, O., Nicol, E. J., Holczer, K. & Grüner, G. Conductivity coherence factors in the conventional superconductors Nb and Pb. *Phys. Rev. B* **50,** 6307–6316 (1994).
15. Ando, Y. *et al.* Metallic in-plane and divergent out-of-plane resistivity of a high-Tc cuprate in the zero temperature limit. *Phys. Rev. Lett.* **77,** 2065–2068 (1996).
16. Dordevic, S. V. *et al.* Global trends in the interplane penetration depth of layered superconductors. *Phys. Rev. B* **65,** 134511 (2002).
17. Basov, D. N., Timusk, T., Dabrowski, B. & Jorgensen, J. D. *c*-axis response of $YBa_2Cu_4O_8$: A pseudogap and possibility of Josephson coupling of CuO_2 planes. *Phys. Rev. B* **50,** 3511–3514 (1994).
18. Homes, C. C., Timusk, T., Bonn, D. A., Liang, R. & Hardy, W. N. Optical properties along the *c* axis of $YBa_2Cu_3O_{6+x}$, for $x = 0.50 \rightarrow 0.95$: Evolution of the pseudogap. *Physica C* **254,** 265–280 (1995).
19. Schützmann, J., Tajima, S., Miyamoto, S. & Tanaka, S. *c*-Axis optical response of fully oxygenated $YBa_2Cu_3O_{7-\delta}$: Observation of dirty-limit-like superconductivity and residual unpaired carriers. *Phys. Rev. Lett.* **73,** 174–177 (1994).
20. Basov, D. N. *et al.* Sum rules and interlayer conductivity of high-T_c cuprates. *Science* **283,** 49–52 (1999).
21. Tanner, D. B. *et al.* Superfluid and normal-fluid densities in high-T_c superconductors. *Physica B* **244,** 1–8 (1998).
22. Orenstein, J. *et al.* Frequency- and temperature-dependent conductivity in $YBa_2Cu_3O_{6+x}$ crystals. *Phys. Rev. B* **42,** 6342–6362 (1990).
23. Shibauchi, T. *et al.* Anisotropic penetration depth in $La_{2-x}Sr_xCuO_4$. *Phys. Rev. Lett.* **72,** 2263–2266 (1994).
24. Lawrence, W. E. & Doniach, S. in *Proc. 12th Int. Conf. Low Temperature Physics* (ed. Kando, E.) 361 (Academic, Kyoto, 1971).
25. Bulaevskii, L. N. Magnetic properties of lamellar superconductors with weak interaction between the layers. *Sov. Phys. JETP* **37,** 1133–1139 (1973).
26. Ambegaokar, V. & Baratoff, A. Tunneling between superconductors. *Phys. Rev. Lett.* **10,** 486–489 (1963).
27. Hardy, W. N., Bonn, D. A., Morgan, D. C., Liang, R. & Zhang, K. Precision measurements of the temperature dependence of λ in $YBa_2Cu_3O_{6.95}$: Strong evidence for nodes in the gap function. *Phys. Rev. Lett.* **70,** 3999–4002 (1993).
28. Shen, Z.-X. *et al.* Anomalously large gap anisotropy in the *a*-*b* plane of $Bi_2Sr_2CaCu_2O_{8+\delta}$. *Phys. Rev. Lett.* **70,** 1553–1556 (1993).
29. Chakravarty, S., Sudbo, A., Anderson, P. W. & Strong, S. Interlayer tunneling and gap anisotropy in high-temperature superconductors. *Science* **261,** 337–340 (1993).

Supplementary Information accompanies this paper on **www.nature.com/nature**.

Acknowledgements We thank A. Chubukov, P. D. Johnson, S. A. Kivelson, P. A. Lee, D. B. Tanner, J. J. Tu, Y. Uemura and T. Valla for discussions. Work in Canada was supported by the Natural Sciences and Engineering Research Council of Canada, and the Canadian Institute for Advanced Research. The $HgBa_2CuO_{4+\delta}$ crystal growth work at Stanford University was supported by the Department of Energy's Office of Basic Energy Sciences, Division of Materials Sciences and Engineering. Work at the University of California at San Diego was supported by the National Science Foundation and the Department of Energy. Work at Brookhaven was supported by the Department of Energy.

Competing interests statement The authors declare that they have no competing financial interests.

Correspondence and requests for materials should be addressed to C.C.H. (homes@bnl.gov).

Magnetic phase control by an electric field

Thomas Lottermoser[1], Thomas Lonkai[2,3], Uwe Amann[2,4], Dietmar Hohlwein[2,3], Jörg Ihringer[2] & Manfred Fiebig[1]

[1]*Max-Born-Institut, Max-Born-Straße 2A, 12489 Berlin, Germany*
[2]*Institut für Angewandte Physik, Universität Tübingen, Auf der Morgenstelle 10, 72076 Tübingen, Germany*
[3]*Hahn-Meitner-Institut, Glienicker Straße 100, 14109 Berlin, Germany*
[4]*Institut Laue-Langevin, 6 Rue Jules Horowitz, BP 156 - 38042 Grenoble Cedex 9, France*

The quest for higher data density in information storage is motivating investigations into approaches for manipulating magnetization by means other than magnetic fields. This is evidenced by the recent boom in magnetoelectronics and 'spintronics'[1], where phenomena such as carrier effects in magnetic semiconductors[2] and high-correlation effects in colossal magnetoresistive compounds[3] are studied for their device potential. The linear magnetoelectric effect—the induction of polarization by a magnetic field and of magnetization by an electric field—provides another route for linking magnetic and electric properties. It was recently discovered that composite materials and magnetic ferroelectrics exhibit magnetoelectric effects that exceed previously known effects[4,5] by orders of magnitude[6–10], with the potential to trigger magnetic or electric phase transitions. Here we report a system whose magnetic phase can be controlled by an external electric field: ferromagnetic ordering in hexagonal $HoMnO_3$ is reversibly switched on and off by the applied field via magnetoelectric interactions. We monitor this process using magneto-optical techniques and reveal its microscopic origin by neutron and X-ray diffraction. From our results, we identify basic requirements for other candidate materials to exhibit magnetoelectric phase control.

Hexagonal $HoMnO_3$ displays ferroelectric ordering at Curie temperature $T_C = 875$ K (ref. 11), antiferromagnetic Mn^{3+} ordering at Néel temperature $T_N = 75$ K (ref. 12), and magnetic Ho^{3+} ordering at $T_{Ho} = 4.6$ K (ref. 13). The ferroelectric phase possesses $P6_3cm$ symmetry and a polarization $P_z = 5.6\,\mu C\,cm^{-2}$ (ref. 11) along the hexagonal *z* axis. Figure 1 shows that it is made up by three magnetic sublattices with Mn^{3+} ($3d^3$) ions at 6c positions and Ho^{3+} ($4f^{10}$) ions at 2a and 4b positions[14]. Anisotropy confines the Mn^{3+} spins to the basal *x*–*y* plane where frustration leads to four possible triangular antiferromagnetic structures[12,15]. In contrast, the Ho^{3+} sublattices are assumed to order Ising-like along *z* showing antiferromagnetism or ferri-/ferromagnetism according to Table 1.

Magnetic Mn^{3+} ordering was monitored by optical second harmonic generation (SHG) as detailed elsewhere[12,15]: Light at frequency ω is incident on a crystal, inducing an electromagnetic polarization at frequency 2ω, which acts as source for a SHG light wave emitted from the crystal. The magnetic symmetry determines the polarization $\mathbf{P}(2\omega)$ of the SHG wave relative to that of the fundamental wave at ω, so that in turn $\mathbf{P}(2\omega)$ reveals the underlying arrangement of Mn^{3+} spins. The relation between SHG polarization and Mn^{3+} ordering is tabulated elsewhere[12,15]. Magnetic Ho^{3+} ordering was monitored by neutron powder diffraction and optical Faraday rotation, that is, the rotation $\Phi \propto \mathbf{B}$ of the plane of polarization of linearly polarized light by the magnetic field $\mathbf{B}$ in a transmission measurement. The microscopic mechanisms driving magnetoelectric phase control were revealed by neutron and X-ray powder diffraction.

Optical measurements were performed at the MBI on flux-grown, polished, *z*-oriented $HoMnO_3$ platelets (~50 μm thick) using previously described transmission set-ups[15,16]. The static